SEGMENTATION OF LASER SURFACES

Bea Csathó[1], Kim Boyer[2], and Sagi Filin[1]

[1] Geomatics Laboratory for Ice Dynamics
Byrd Polar Research Center, OSU,
csatho.1@osu.edu, filin.1@osu.edu
[2] Signal Analysis and Machine Perception Laboratory
Department of Electrical Engineering, OSU
kim@ee.eng.ohio-state.edu

KEY WORDS: Segmentation, surface parameterization, waveform analysis, sequential estimators

ABSTRACT

Laser scanning systems provide raw surface points, that is x, y, z coordinates for each laser footprint. To obtain an explicit description of the surface to be mapped, such as breaklines or surface patches that can be analytically described, the raw laser surface should be segmented. The segmented surface is more suitable for further analysis, such as object recognition and surface matching. However, the segmentation of laser surfaces is not an easy task. The error distribution is non-Gaussian, more likely a thick-tailed distribution contaminated by outliers. Outliers result from laser reflections on object boundaries or steep surfaces. The true underlying surface model is rarely known before hand and it might be different from the visible surface since the laser energy can penetrate vegetation or water. We propose to use an autonomous, statistically robust, sequential function approximation approach to segment the surface into surface patches that can be described analytically. Its core is the Robust Sequential Estimator, a robust extension to the method of sequential least squares. Unlike most existing surface characterization techniques, this method generates complete surface hypotheses in parameter space. Given a noisy set of raw laser points, the algorithm first selects appropriate seed points representing possible surfaces. For each nonredundant seed it chooses the best approximating model from a given set of competing models. With this best model, each surface is expanded from its seed over the entire area to find all points of that particular surface. In the final step, the ambiguities are resolved and the isolated points are removed. The end result is a set of parameterized surfaces and their boundaries. We work with two models, planar and biquadratic, because they approximate most natural and man-made surfaces well. The segmentation may be followed by the joint inversion of the laser waveforms over the given surface patch to refine and verify the surface model. Synthetic and real laser surfaces are used to demonstrate the segmentation concept.

1 Introduction

Range information provides a basic, fundamental contribution toward the understanding and reconstruction of 3-D shape, which is required for general purpose object recognition and image understanding. The goal of segmentation is to make surface properties explicit. Surface properties include explicit description of discontinuities, description of piecewise continuous surface patches, and other surface properties, such as surface roughness, and reflectivity. Segmentation also provides input for data fusion, object recognition and change detection.

Surface segmentation algorithms have extensively being used in computer vision (e.g., [Besl, 1988]). Segmentation organizes the surface points into spatially coherent surface primitives by using low-level processes as well as generic information. In this fashion a precise, general and compact symbolic representation of the original point set is created without using high-level, object information. The various surface segmentation approaches in computer vision have not yet fully exploited in the processing Airborne Laser Ranging (ALR) data. Here, usually data or application specific, often proprietary data thinning and blunder detection procedures are followed immediately by model based object recognition.

First we provide some background on surface segmentation followed by specifics of the surfaces and laser point sets considered in ALR. Then a robust, sequential surface segmentation approach [Boyer et al., 1994] is presented in detail. We recommend this procedure as a part of a multisensor (e.g., laser, stereo, multispectral) object recognition process, that includes the following steps:

- Preprocessing of sensory data, geometric and radiometric corrections.
- Transformation of surface points measured by laser and stereo into a common reference system.
- Segmentation and feature extraction of surfaces and imagery. Each data set can be processed individually. On the other hand it may be advantageous to combine the data for providing an explicit description of surface properties for example by classification [Csathó et al., 1999]
- Grouping and model based object recognition.

2 Background on object recognition from digital surfaces

2.1 Range image understanding in computer vision

The literature on automated surface model construction from 3D point sets contains two main paradigms [Hoover et al., 1998]. In the mesh paradigm, a triangular-patch or regular grid surface model is constructed from laser points, followed by the selection of a subset of the vertices. The selected vertices determine a polygonal surface which approximate the original data within predetermined error bars. A variety of methods have been explored for the purpose of

simplifying surfaces. For a good overview of the topic the interested reader is referred to [Heckbert and Garland, 1997].

In the Surface Adjacency Graph (SAG) paradigm, the points are segmented into regions by fitting analytical surfaces to the corresponding surface patches. An example of the application of this paradigm is the region growing based on variable-order surface fitting, such as the algorithm described in this paper.

2.2 Object recognition from laser scanning

Pre-processing, involving the computation of the laser footprint from the GPS, INS and laser range data, is usually followed by thinning and manual editing to reduce the size of the data stream and to remove the outliers. Then the cloud of almost randomly distributed laser points is separated into ground and non-ground returns by using low-level processing, such as histogram thresholding, morphological filtering, and the application of autoregressive integrated processes ([Lindenberger, 1993], and [Kraus and Pfeifer, 1998]). Instead of segmenting the whole surface into surface primitives, the low-level processing is usually immediately followed by model based object recognition and reconstruction of certain type of objects, for example buildings (e.g., [Axelsson, 1999] and [Maas and Vosselman, 1999]).

To facilitate the automation of the object recognition and image understanding process many authors recommend the inclusion of other sensory data into the process. The redundant and complementary information from stereo photogrammetry, multi(hyper) spectral imagery, and other sources can be fused at the different points of the processing chain for detection, and classification of features and objects, for surface and objects reconstruction, and for error detection. For example [Haala and Brenner, 1999] achieve automatic detection of topographic features by combining laser data and color imagery in a classification step, and uses laser data and 2D ground plan information to obtain 3D reconstruction of buildings.

3 Segmentation and object recognition for different applications

An ideal segmentation would partition the surface points into surface primitives without making any domain-dependent assumptions about specific objects, object classes, or applications [Besl, 1988]. In reality, the selection of the best segmentation algorithm is application dependent. The sensor characteristics, type of the measured quantities, the spatial distribution of the laser points, the object properties, the error distribution, and the purpose of the survey all should be considered.

Algorithms using surface fitting work well when recognition of man-made objects, such as buildings, roads, etc., is the major goal. These are smooth and solid objects usually bounded by planar surfaces. The texture of surfaces (for example tiles on a roof, or vegetation on topographic surfaces) are treated as additional random noise superimposed on the smooth surface.

Segmentation of natural surfaces, such as sea ice, ice sheet or land may pose different problems. These surfaces are viewed as a combination of deterministic and stochastic parts. In many applications, for example in geology and glaciology, the statistical character of the surface (the stochastic part), is also a subject of investigation. Surface texture statistics, like surface roughness or correlation length can be the basis of segmentation. Alternatively they can be used as additional clues for object recognition.

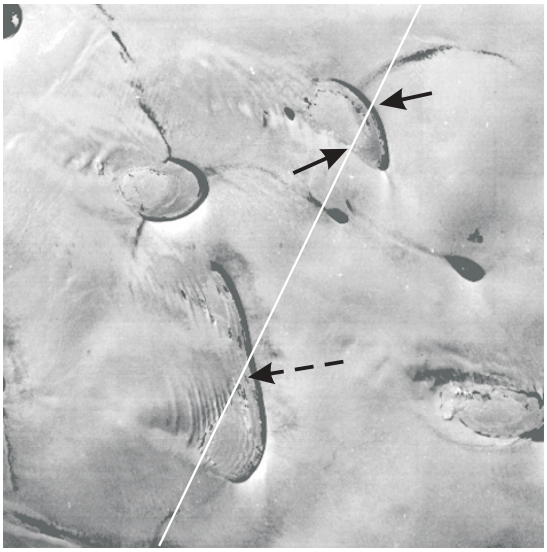

Figure 1: Aerial photograph of ice sheet surface with superglacial lakes. The elevation profile in Figure 2 is extracted along the white line. Solid arrows marks lake boundaries and the dashed arrow points to ripples.

Consider for example the area of superglacial lakes and complicated drainage patterns on the Greenland ice sheet (Figure 1 and Figure 2(a). Although surface fitting is the logical solution for describing the overall shape, ice sheets are so simple that most of the object types can directly be recognized by using simple clues, such as roughness and slope. Figure 2 illustrates how scale-space analysis of the elevation profiles as well as its first and second derivatives renders the lakes. Lakes are horizontal and smooth, therefore the derivatives of the surface elevation are small (for example see the lake in Figure 1 and Figure 2, between the solid arrows). The ripple zones, that is the series of bumps contouring the lake shores down-glacier (for example around dashed arrow in Figure 1), have large surface roughness resulting large and rapidly alternating derivatives (Figure 2(b)-(c)). To suppress this fine scale information the elevation profile was smoothed by convolution with Gaussian kernels of increasing width. The second derivatives of the smoothed elevation profiles was inspected to select the best scale for rendering the lake boundaries (Figure 2(d)).

A somewhat related topic is the determination of surface statistics from a set of laser points or laser waveform. For horizontal, random rough surfaces where the roughness scale is much smaller than the footprint, the surface roughness within each footprint can be estimated from the pulse width of the return waveform [Gardner, 1992]. This approximation is valid for some natural surfaces, like sea ice and for large footprint laser system (LVIS, ICESAT). For more complicated surfaces the approach introduced by [Goff and Jordan, 1988] might be followed. He modeled the ocean floor as an anisotropic, zero-mean, Gaussian random field to recover second order statistics, namely amplitude, orientation, characteristic wave numbers and Hausdorff (fractal) dimension of seafloor topography from Sea Beam (sonar) data.

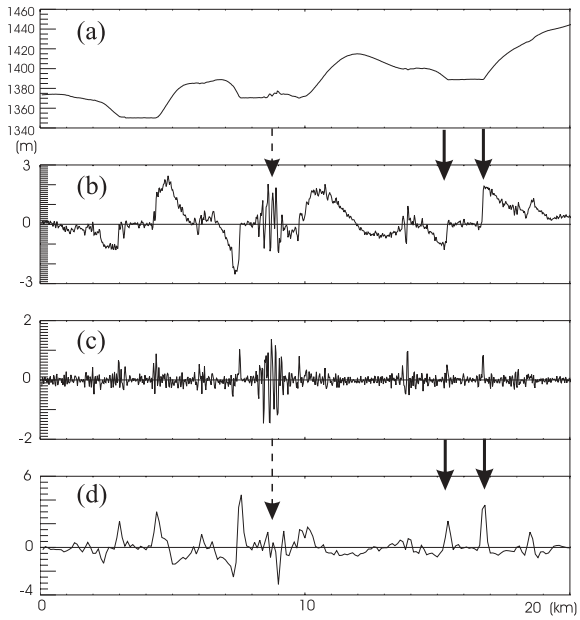

Figure 2: Object recognition from surface elevation and roughness on laser altimetry profile in the area depicted in Fig. 1. Solid arrows mark lake boundaries and the dashed arrow points to a ripple zone. (a) Surface elevation from airborne laser profiling, (b) first, and (c) second derivatives, and (d) second derivative of elevation profile smoothed by convolution with a Gaussian kernel.

4 Error model of ALR

The 0.1-0.2 m accuracy of ALR provided by the service providers [Flood, 1999] and investigators (e.g., [Krabill et al., 1995]) refers for flat or gently sloping surfaces, low to medium flight height, and for objects with high surface reflectivity. In this "ideal' case, the height accuracy consists of a 0.05-0.15 m fairly constant error from GPS and laser ranging (for GPS baselines shorter than say 100 km), and an error of ca. 0.5-2 cm per 100 m of flying height for typical attitude errors and a scan angle of 30 ^{o} [Baltsavias, 1999]. [Schenk et al., 1999] examines the resulting surface errors for horizontal and sloped surfaces. His simple error analysis demonstrates that the errors are complicated functions of topography, flight direction and the systematic positioning and attitude determination errors.

No comprehensive analysis has been attempted yet for quantifying the error of ALR for complex, 3D surfaces. It is known that larger errors tend to appear along vertical and steep object boundaries since the same planimetric error manifests in larger elevation error on steep slopes than on flat surfaces. There is also an increase in ranging error where abrupt changes in elevation and surface normal occur within the laser footprint. This error depends on several factors, such as the ranging principle used by the laser system, the distribution of the elevations within the footprint, and the background noise. [Gardner, 1992] uses closed form equations of the laser return waveforms to describe the increase of the ranging error on sloping or random rough surfaces caused by the pulse broadening. His result is supported by the observations of [Kraus and Pfeifer, 1998] who report that with increasing terrain slope and roughness, the height accuracy deteriorates to 0.5-1 m for 1000 m flying height.

These results suggest that the surface error of ALR has non-Gaussian distribution. Larger errors, possibly outliers are expected for example on steep slopes and along object boundaries.

5 Robust segmentation algorithm

In this paper we present an autonomous, statistically robust, sequential estimator (RSE) approach to simultaneously parameterize and organize laser surfaces. Details of the procedure, including the mathematical background, has been published in [Boyer et al., 1994]. The approach is recommended for the segmentation of noisy, outlier-ridden (not Gaussian) laser points into smooth surface patches. Unlike most existing techniques, this method creates complete surface hypotheses.

5.1 Mathematical model

We assume that surface elevations $z_i = (x_i, y_i)$ are measured by ALR at n arbitrary locations. Then, a general linear regression model fitting a (generally nonlinear) function of p parameters can be written as:

$$z_i = x_{i,1}\theta_1 + ... + x_{i,p}\theta_p + \epsilon_i \qquad (1)$$

for $i = 1, ..., n$, where ϵ_i represents a disturbance (error, noise) in the observation. For example, with $p = 6, x_{i,1} = 1, x_{i,2} = x_i, x_{i,3} = y_i, x_{i,4} = x_i y_i, X_{i,5} = x_i^2, x_{i,6} = y_i^2$, and with $\theta_1 = a, \theta_2 = b$, and so on, we can fit a function of the form:

$$f(x, y) = a + bx + cy + dxy + ex^2 + fy^2 \qquad (2)$$

In matrix notation, eq. 1 is represented as follows:

$$z = X\theta + \epsilon \qquad (3)$$

where z is an n-vector of observations on the dependent variable (elevation), X is an $n \times p$ matrix of observation on the explanatory variable (the horizontal coordinates of the observations and their polynomials) having rank p, θ is a p-vector of parameters to be estimated (parameters of fitted surfaces), and ϵ is an n-vector of disturbances (errors in elevation)

Only planar and biquadratic surfaces can be fitted in the current implementation of the algorithm. However, the algorithm is general and can be, in principle, extended to any number of parameters. Based on the arguments presented in Section 4 we assume that the error distribution of ALR data is non-Gaussian and contaminated by outliers around object boundaries. Since heavy tailed error distributions are reasonably represented by a t(Student)-distribution, a t-distribution having degree of freedom f and scaled by a parameter σ was chosen as a stochastic model.

5.2 Preprocessing of ALR data

The preprocessing involves the computation of the laser footprint position in a global, geographic coordinate system. Details on how to establish the relationship between the laser range and the attitude and position of the aircraft are given for example in [Vaughn et al., 1996]. We omit here these details and assume that the positions of the laser footprints in a Cartesian coordinate system are made available for the segmentation.

Interpolation The RSE algorithm like most other segmentation algorithms has originally been developed for close-range applications and it works on range images rather than a

cloud of 3-D points having no topological relationship. Therefore the raw laser data should be interpolated into a regular grid on the xy plane prior to segmentation. Owing to the quasi random distribution of the laser points the interpolation errors are usually large, especially near breaklines.

ALR data acquired by the Airborne Topographic Mapper conical scanner [Krabill et al., 1995] at the Commission III test site in Ocean City, MD ([Csathó et al., 1998]) are used to illustrate some of the problems (Figure 3). Figure 3(b) shows the distribution of the laser points in 2D. The contour map is created by using a TIN model based interpolation. In addition to the distribution of the laser points let us consider the location of the laser system relative to the building. The aircraft passed the building on its left, so the laser was firing from the left producing illuminated footprints on the ground, on the roof on the building and on the walls. Small segments of two scans are marked by gray squares and circles in Figure 3(b). A few laser points are located on the wall which is close to the sensor (left side in (b) and front of building in (a)), and there is some occlusion on the opposite side (right side in (b)). The distribution of the laser points on the near side is quite irregular, probably owing to the irregular outline of the building and the balconies (Figure 3(a)).

The surface depicted in Figure 3(c) is interpolated by using minimum curvature spline interpolation. This method minimizes the total curvature and the surface is not allowed to bend sharply. This results overshooting at corners or along edges (Note the peaks around the roof of the building). Figure 3(d) shows the surface interpolated by using a TIN model based linear interpolation. The TIN model provides a better, but visually not very pleasing solution. The resulting triangles give a tent like appearance, moreover many points interpolated along the side of the building have large elevation errors [Schenk et al., 1999].

5.3 The procedure

After the preprocessing and interpolation the data are segmented by a robust sequential estimator (RSE) procedure. The major steps of the RSE approach are summarized in Fig. 4.

The algorithms first selects appropriate seed points that represent possible surfaces. For each nonredundant seed it chooses the best approximation from the selection of planar and biquadratic models, using a modified Akaike Information Criterion. With this best model, each surface is expanded from its seed over the entire image; this step is repeated for all seeds. The most significant and novel features of the algorithm, the seed selection, model choice and expand operations are embedded in a loop. The procedure starts with stringent criteria for smoothness and minimum size of the seed regions and the thresholds are decreased in every iteration. The seed selection stops when all data is assigned to at least one surface. The remaining steps of pruning, removing and filling are simple postprocessing heuristics. The procedure ends with organizing the regions into a complete, non-ambiguous scene description.

5.4 Seed selection

Ideally, seed regions are selected within every independent surface. Redundant seeds increase the computational burden and risk of over segmentation, while missing seeds could leave surfaces unmodeled. Surface fitting for region growing starts in every seed region. There are different approaches for

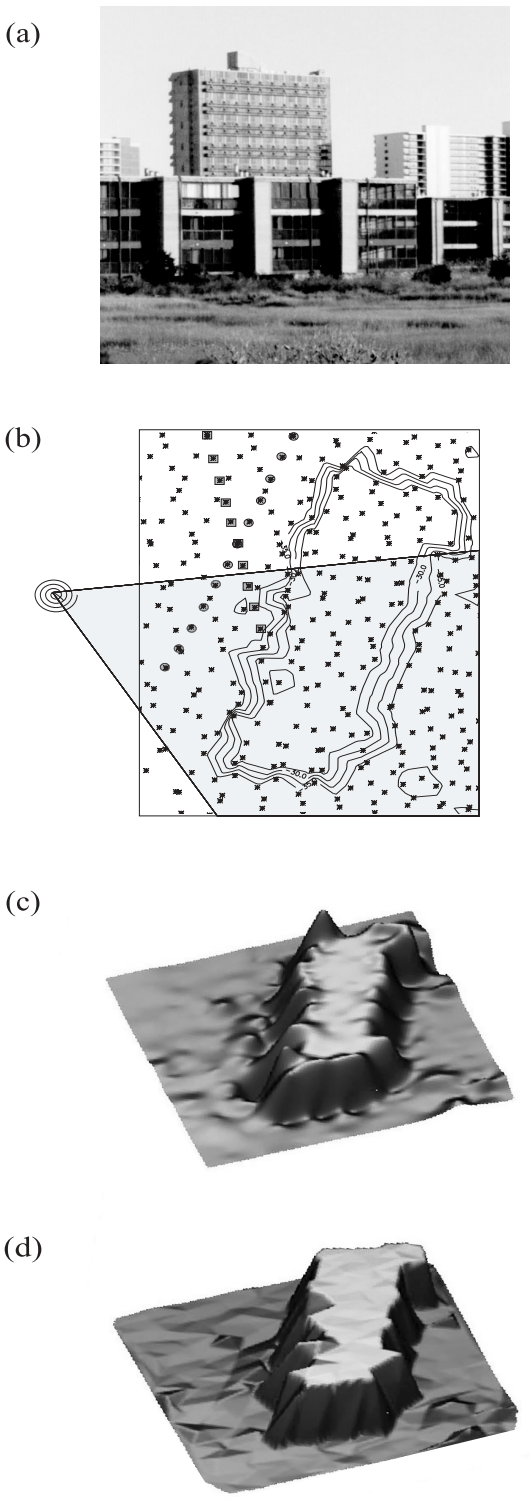

Figure 3: Interpolation of laser points. (a) Photograph of the building, (b) Contour map of the building from laser points using TIN model based linear interpolation, square and circle mark laser footprint belonging to the same scan line, spiral shows the perspective center of the photograph in (a), (c) interpolation of laser data by minimum curvature method, (d) interpolation of laser data by linear interpolation of TIN model.

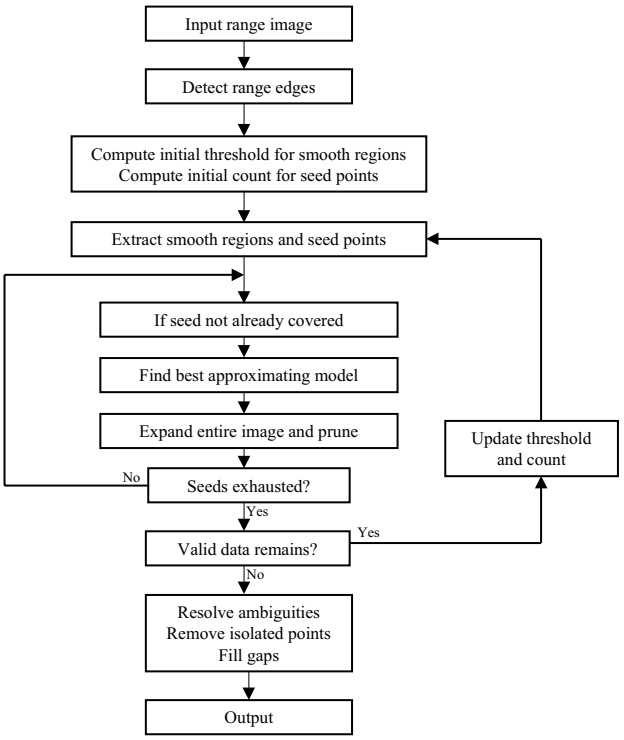

Figure 4: Block diagram of complete robust surface perception scheme

seed selection. For example [Besl, 1988] extracts connected regions from the HK-sign map (mean and Gaussian curvatures), and erodes these regions until sufficiently small regions remain. By a seed point, we mean the center of the seed window. In the RSE approach, first simple 2D edge detector is used to locate smooth regions. Points which are centers of the largest, contiguous regions, are identified. Finally, redundant seeds are eliminated. The procedure is implemented in a loop, starting with stringent criterias for smoothness and minimum size of smooth regions. These thresholds are decreased in every iteration. Seed selection stops when all the data have been covered by at least one surface, except for isolated singletons and pairs, or when no smooth region left.

5.5 Choosing best approximating model

The next step is to choose the best approximating model from planar and biquadratic models for each seed point. In this subsection first the robust M-estimator, the Robust Sequential Estimator (RSE), and the information theoretic model selection is introduced briefly followed by the description of the procedure used for selecting the best approximating model.

Robust M-Estimator Robust estimators are more efficient (lower variance) than least squares (LS) if the errors are not normally distributed, as is the case in laser scanning. They are only slightly less effective than LS if the error has normal distribution. We use a maximum likelihood (M)-estimator as a robust estimator for the t distribution error model that we assume for the ALR data (Section 4). Unfortunately, the direct evaluation of maximum likelihood estimates from non-normal distributions becomes quite complicated. Therefore, estimates are obtained by using iteratively reweighted least squares (IRLS). Let $p(\epsilon_i)$ be any differentiable error density function which can be written in the form

$$p(\epsilon_i)\ \alpha\ \sigma^{-1} g\{(\frac{\epsilon_i}{\sigma})^2\} \tag{4}$$

where σ is the scale parameter, $g\{.\}$ denotes a functional form, and $\epsilon_i = z_i - \sum_j \theta_j x_{i,j}$ is the i^{th} actual error from eq.1. After computing the log-likelihood for θ and σ^2 we get a set of nonlinear equations. These nonlinear equations can be solved using IRLS. Rewriting the equations in matrix form

$$X^T W(z - X\hat{\theta}) = 0 \tag{5}$$

where W is a diagonal weight matrix whose elements depend on the residuals, since

$$w_i = w_i(\theta, \sigma^2) = -2[\frac{\partial \ln g(\xi)}{\partial \xi}]_{\xi=(\epsilon_i/\sigma)^2} \tag{6}$$

The resulting iterative scheme, after simplification, is given by

$$\hat{\theta}_k = \hat{\theta}_{k-1} + (x^T W_{k-1} X)^{-1} X^T W_{k-1}(z - X\hat{\theta}_{k-1}) \tag{7}$$

For a t distribution having a degree of freedom f and scaled by a parameter σ

$$g[(\epsilon_i/\sigma)^2] = [1 + \epsilon_i^2/(f\sigma 2)]^{(-1/2)(1+f)} \tag{8}$$

Substituting this expression for g in (6) yields the individual weights:

$$w_i = \frac{1+f}{f + (r_i/s)^2} \tag{9}$$

where the residual $r_i = z_i - \sum_j \hat{\theta}_j x_{i,j}$. We use s in this expression to distinguish the (unknown) true value of the scale parameter, σ, from an estimated value, s, used in computing the weights. These weights are then assigned to the diagonal elements of the weighting matrix, W, and (7) is used to update the parameters.

Robust Sequential Estimator (RSE) The RSE is a robust extension of the sequential least squares (SLS) estimator. The RSE can be applied to any linear regression model of the type defined in (1). In the SLS algorithm, equal weights are assigned to every data point, while the RSE differentiates between valid data and outliers through its weighting mechanism. That is, the RSE rejects any data point which fails to qualify as possibly valid for the current surface model. The RSE does not remove these data points from the data set entirely - just from the current surface. The estimation starts from an initial robust estimate of the surface parameters in a small neighborhood centered around a seed point. The parameters of the fitted surface are computed by IRLS with errors assumed to be t distributed. The RSE then adds the remaining data sequentially, assigning weights to each new observation based on the previous surface estimate.

Information theoretic model selection We have to choose the best approximating model from a given set of models before we can apply the RSE. Since models with more parameters fit the data better, the selection criteria should balance complexity with goodness of fit. The Akaike Information Criterion (AIC) is a powerful tool for choosing among different regression models. The asymptotically consistent AIC (CAIC)is a generalization of the Akaike Information Criterion (AIC) by making it asymptotically consistent and by penalizing over parameterization more stringently to avoid modeling

the noise. If we assume that the errors in the general regression model are independent and identically t-distributed, the CAIC is given by

$$CAIC = -2(1+f)/2 \sum_{i=1}^{n} w_i log[1 + \frac{r_i^2}{f\sigma^2}] + p(log(n)+1) \quad (10)$$

where the first part describes the log-likelihood of the model with p parameter, $log(n)+1$ is the cost of fitting an additional parameter, n is the number of observations, and w_i and r_i are the corresponding weight and residual for the ith observation. For a fixed data set it is easy to compare the CAIC for different fitted surfaces. However, with a sequential approach the data set is not fixed. Since CAIC assumes a fixed data set, we start the RSE algorithm in a local fixed window, and compute the parameter vector using IRLS. From this estimate, we compute the initial CAIC. Then the RSE expands the initial window, until it encounters outliers. To compute the modified, asymptotically consistent Akaike information criterion (MCAIC) the CAIC is normalized by the total number of observations in the final, maximal window for each model:

$$MCAIC = K \frac{initialCAIC}{N} \quad (11)$$

where K is an arbitrary constant, we use the number of points in the initial window.

To select the best candidate model for each candidate model the following procedure is used:

- For each seed point robust parameter estimates are obtained for each candidate model.
- The initial value of CAIC is computed by using (10).
- Points are added sequentially by expanding the initial window in four direction, updating the parameter estimates by using RSE. A point is considered as outlier if its weight falls below a threshold. If the ratio of outliers to total data points exceeds 75 percent on a side, the window is not expanded further in this direction.
- For each model and its resulting window, the MCAIC is computed by using (11). For this seed, the model minimizing MCAIC is selected as the best approximating model.

5.6 Postprocessing

Expand The expand procedure is employed both as part of the seed selection-model selection loop, and to establish the final model parameters and the set of points supporting that particular parameter vector. Once we have the best approximating model for a surface (seed), we use this model and let the surface grow over the entire scene. This process is repeated for all surfaces at the appropriate seed points using the best approximating models as obtained in the **choose** step.

Prune The expand process may assign isolated points to a surface. Those with fewer then 2 co-surface 8-neighbors are assigned to the base surface.

Resolve For the end of the segmentation each laser point should be assigned to one surface only. To resolve the ambiguities a 5 by 5 neighborhood of each ambiguous point is examined by calculating the average estimator weight for each candidate surface. The surface yielding the maximum average weight is selected.

Remove (re-prune) After the resolve step, some points which were not isolated prior to resolution, may become isolated. These points are removed by re-pruning.

Fill At this point the surface usually have pinholes where points are assigned to the base surface within another surface. This is the dual of the isolated point problem. The final assignment of these points is based on their 8-neighborhood.

The **final output of the segmentation** is:

- 3D graph surface equations,
- 2D region boundary equations,
- fit error,
- other characteristics of surface patches.

5.7 Experimental results

Experiments on both synthetic data and real range imagery are presented in [Boyer et al., 1994] to demonstrate the performance of the RSE segmentation.

Figure 5-6 shows the result of one of these experiments. The synthetic surface has two planar region with smooth transitions into a cylindrical joining region such that depth and orientation is continuous everywhere (Figure 5(a)). Noise and outliers were added to simulate a noisy set of range data Figure 5(b). Surfaces with smooth joins are more difficult to segment but the algorithms addresses this case reasonably well. The recovered surfaces and the segmentation boundaries are shown in Figure 6.

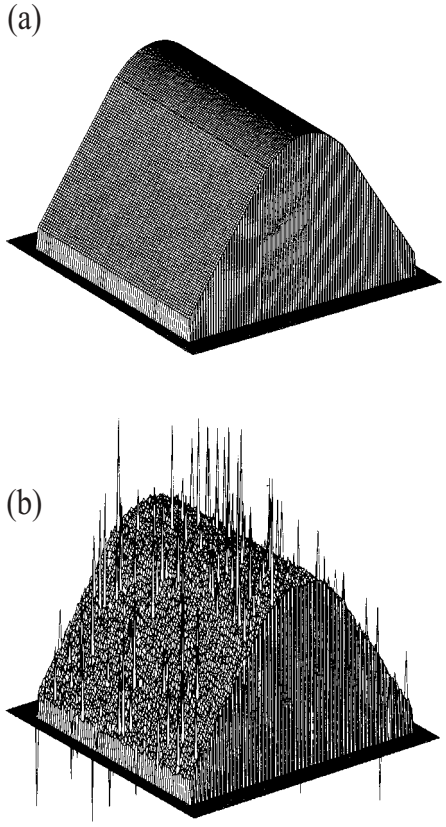

Figure 5: (a) Smooth join surface and (b) surface contaminated with added Gaussian noise and outliers

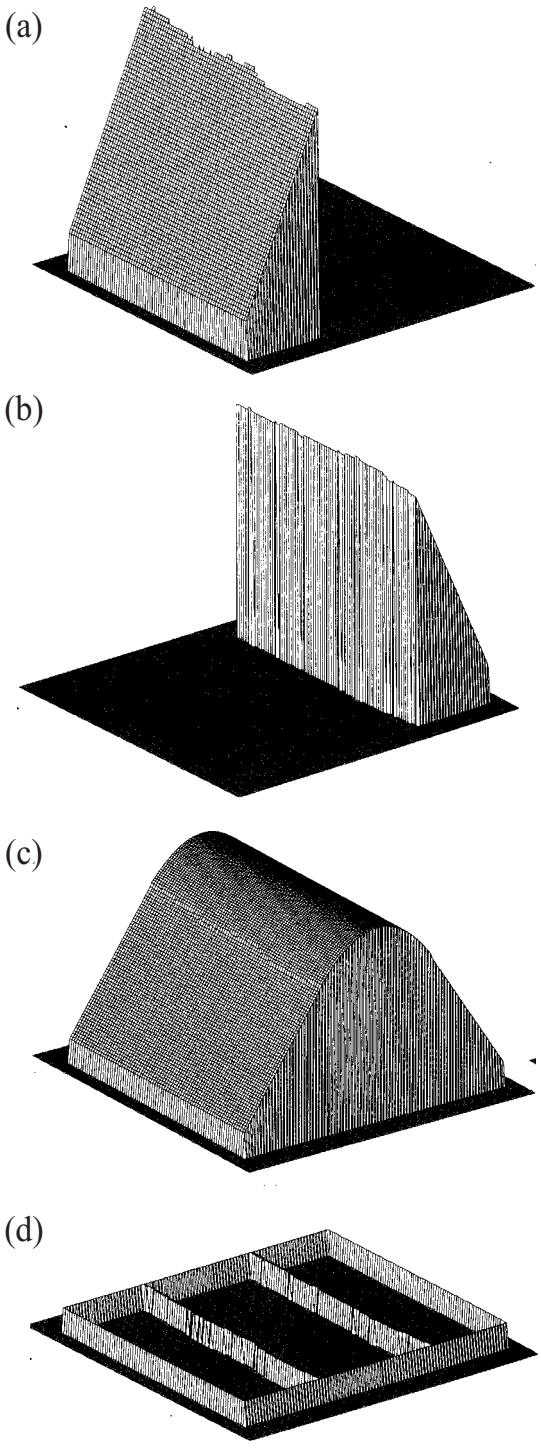

Figure 6: Recovered surfaces and segmentation (a) Plane1, (b) Plane2, (c) all three surfaces, (d) segmentation boundaries

6 Discussion and conclusions

Airborne laser scanning is an increasingly popular data acquisition method for generating DTMs. It samples the surface at high a density and the range measurements are very accurate. However, the raw laser points are not a meaningful description of the surface because the major surface characteristic, such as breaklines, formlines, smooth surface patches, and surface roughness, are not explicitly encoded. Surface segmentation attempts to extract this information from the cloud of 3-D laser points. We have proposed a region growing segmentation method that takes the stochastic nature of laser points into account and it is robust regarding blunders. We are currently extending the approach to process directly irregularly distributed data sets in order to avoid gridding as a pre-process.

Segmenting laser points into meaningful surface patches would greatly benefit from additional information. Usually, laser data sets consist of a (huge) list of 3-D points. It is conceivable to record additional information, for example the entire waveform of the returning laser signal, or the scene brightness. Waveform analysis and analyzing scene brightness could be incorporated into the segmentation process.

For region-growing segmentation to be successful, a sufficient number of points per surface patch is required. This is usually the case for airborne laser data sets. Since the segmentation identifies smooth surface patches, breaklines and formlines are defined by region boundaries. Sometimes, the region boundaries do not determine breaklines well, however. This is an inherent problem with laser data sets; the spatial distribution of footprints may be considered a random sampling as far as object boundaries are concerned. It would be sheer coincidence if a footprint would coincide with an object boundary, say a building outline. Even if it did we would not know. If object boundaries are important for a particular application, other sources but laser ranging may be required. For example, stereo photogrammetry allows direct determination of 3-D object boundaries. Therefore, it makes sense to combine the strengths of different sensors.

7 Acknowledgements

The example with the Greenland ice sheet is from the ICESAT project, funded by the NASA [Csathó et al., 1995]. Other examples used in this paper are from the Ocean City test site, established by ISPRS WG III/5 [Csathó et al., 1998].

REFERENCES

[Axelsson, 1999] Axelsson, 1999. Processing of laser scanner data – algorithms and applications. *ISPRS Journal of Photogrammetry and Remote Sensing*, Vol. 54, Nos. 2-3, pp. 138-147.

[Besl, 1988] Besl, P. J., 1988. *Surfaces in Range Image Understanding*. Springer-Verlag, New York, 340 pages.

[Baltsavias, 1999] Baltsavias, E. P., 1999. A comparison between photogrammetry and laser scanning. *ISPRS Journal of Photogrammetry and Remote Sensing*, Vol. 54, Nos. 2-3, pp. 83-94.

[Boyer et al., 1994] Boyer, K. L., M. J. Mirza, and G. Ganguly, 1994. The robust sequential estimator: a general approach and its application to surface organization in range data. *IEEE Transactions on Pattern Analysis and Machine Intelligence*, Vol. 16, No. 10, pp. 987-1001.

[Csathó et al., 1995] Csathó, B., A. F. Schenk, R. H. Thomas, and W. B. Krabill, 1995. Topographic mapping by laser altimetry. *Proceedings of SPIE*, Vol. 2572, pp. 10-20.

[Csathó et al., 1998] Csathó, B., W. Krabill, J. Lucas, and T. Schenk, 1998. A multisensor data set of an urban and

coastal scene. *International Archives of Photogrammetry and Remote Sensing*, Vol. 32, Part 3/2, pp. 588-592.

[Csathó et al., 1999] Csathó, B., T. Schenk, D-C. Lee and S. Filin, 1999. Inclusion of multispectral data into object recognition. *International Archives of Photogrammetry and Remote Sensing*, Vol. 32, Part 7-4-3 W6, pp. 53-61.

[Flood, 1999] Flood, M., 1999. Commercial development of airborne laser altimetry - A review of the commercial instrument market and its projected growth. In *International Archives of Photogrammetry and Remote Sensing*, Vol. 32, Part 3 W14, this proceedings

[Gardner, 1992] Gardner, C. S., 1992. Ranging performance of satellite laser altimeters. *IEEE Transactions on Geoscience and Remote Sensing*, Vol. 30, No. 5, pp. 1061-1072.

[Goff and Jordan, 1988] Goff, J. A., and T. H. Jordan, 1988. Stochastic modeling of seafloor morphology: inversion of sea beam data for second-order statistics. *Journal of Geophysical Research*, Vol. 93, No. B11, pp. 13589-13608

[Haala and Brenner, 1999] Haala, N., and C. Brenner, 1999. Extraction of buildings and trees in urban environments. *ISPRS Journal of Photogrammetry and Remote Sensing*, Vol. 54, Nos 2-3., pp. 130-137.

[Heckbert and Garland, 1997] Heckbert, P. S. and M. Garland, 1997. Survey of polygonal surface simplification algorithms. In *SIGGRAPH '97 Course Notes Multiresolution Surface Modeling*, Los Angeles, CA

[Hoover et al., 1996] Hoover, A., G.-Jean Baptiste, X. Jiang, P. J. Flynn, H. Bunke, D. Goldgof, K. Bowyer, D. Eggert, A. Fitzgibbon, and R. Fisher, 1996. An experimental comparison of range image segmentation algorithms. *IEEE Transactions on Pattern Analysis and Machine Intelligence*, Vol. 18, No 7, pp. 673-689.

[Hoover et al., 1998] Hoover, A., D. Goldgof, and K. W. Bowyer, 1998. Dynamic-scale model construction from range imagery. *IEEE Transactions on Pattern Analysis and Machine Intelligence*, Vol. 20, No. 12, pp. 1352-1357.

[Kraus and Pfeifer, 1998] Kraus, K., and N. Pfeifer, 1998. Determination of terrain models in wooded areas with airborne laser scanner data. *ISPRS Journal of Photogrammetry and Remote Sensing*, Vol. 53, No. 4, pp. 193-203.

[Krabill et al., 1995] Krabill, W. B., R. H. Thomas, C. F. Martin, R. N. Swift, and E. B. Frederick, 1995. Accuracy of airborne laser altimetry over the Greenland ice sheet. *International Journal of Remote Sensing*, Vol. 16, pp. 1211-1222.

[Lindenberger, 1993] Lindenberger, J. 1993. Laser-Profilmessung zur topographischen Geländeaufnahme. PhD Dissertation, Deutsche Geodätische Kommission bei der Bayerischen Akademieder Wissenschaften, Reihe C, Heft Nr. 400.

[Maas and Vosselman, 1999] Maas, H-G., and G. Vosselman, 1999. Two algorithms for extracting building models from raw laser altimetry data. *ISPRS Journal of Photogrammetry and Remote Sensing*, Vol. 54, Nos. 2-3, pp. 153-163.

[Schenk, 1999] Schenk, T., 1999. Photogrammetry and laser altimetry. In *International Archives of Photogrammetry and Remote Sensing*, Vol. 32, Part 3 W14, this proceedings

[Schenk et al., 1999] Schenk, T., B. Csathó, and D-C. Lee, 1999. Accuracy study of airborne laser ranging over urban areas. In *International Archives of Photogrammetry and Remote Sensing*, Vol. 32, Part 3 W14, this proceedings

[Vaughn et al., 1996] Vaughn, C., Bufton, J., Krabill, W., and Rabine, D., 1996. Georeferencing of airborne laser altimetry measurements. *International Journal of Remote Sensing*, Vol. 17, No. 11, pp. 2185-2200.